Dissecting the microbial community structure of internal organs during the early postmortem period in a murine corpse model

Ruina Liu
Xi'an Jiaotong University
Kai Zhang
Xi'an Jiaotong University
Huan Li
Xi'an Mental Health Center Hospital
Qinru Sun
Xi'an Jiaotong University
Xin Wei
Xi'an Jiaotong University
Huiyu Li
Xi'an Jiaotong University
Siruo Zhang
Shaanxi Provincial People's Hospital
Shuanliang Fan
Xi'an Jiaotong University
Zhenyuan Wang (wzy218@xjtu.edu.cn)
Xi'an Jiaotong University https://orcid.org/0000-0003-3561-6414

Research Article

Keywords: thanatomicrobiome, body decomposition,16S rRNA, internal organs

Posted Date: May 31st, 2022

DOI: https://doi.org/10.21203/rs.3.rs-1099733/v2

Version of Record: A version of this preprint was published at BMC Microbiology on February 10th, 2023.
See the published version at https://doi.org/10.1186/s12866-023-02786-0.

Abstract

Background

Microorganisms distribute and proliferate both inside and outside the body, which are the main mediators of decomposition after death. However, limited information is available on the postmortem microbiota changes of extraintestinal body sites in the early decomposition stage of mammalian corpses.

Results

This study investigated microbial composition variations among different organs and the relationship between microbial communities and time since death over 1 day of decomposition in male C57BL/6J mice by 16S rRNA sequencing. During 1 day of decomposition, *Agrobacterium*, *Prevotella*, *Bacillus*, and *Turicibacter* were regarded as time-relevant genera in internal organs at different timepoints. Pathways associated with lipid, amino acid, carbohydrate and terpenoid and polyketide metabolism were significantly enriched at 8 hours than that at 0.5 or 4 hours. The microbiome compositions and postmortem metabolic pathways differed by time since death, and more importantly, these alterations were organ specific.

Conclusion

The dominant microbes differed by organ, while they tended toward similarity as decomposition progressed. The observed thanatomicrobiome variation by body site provides new knowledge into decomposition ecology and forensic microbiology. Additionally, the microbes detected at 0.5 hours in internal organs may inform a new direction for organ transplantation.

Background

Decomposition involves a mosaic ecosystem closely related to biotic factors (such as the corpse, insects, and microbes), and abiotic factors (such as temperature and humidity). This process mobilizes nutrients bound to once-living organisms into the surrounding environment, yielding a group of assembled decomposers to realize nutrient recycling [1]. Exploring the action of these organisms, especially microbes, in the maintenance of intrinsic ecosystems is important. We propose that the microbial composition differences seen during decomposition can be directly traced to the status of bacteria present in the earliest stages of decomposition. Microorganisms, important decomposers, are ubiquitous and come from the environment, are scavengers, or were part of the existing microflora of once-living organisms. Briefly after the death of organism, microbes begin to proliferate, transmigrate and produce specialized proteins that digest host tissues [2]. Moreover, volatile organic compounds associated with the process of bacterial metabolism recruit (or repel) insects [3], which, if given the opportunity, can subsequently eliminate any remaining flesh. Thus, understanding the bacterial basis of decomposition is

crucial for understanding decomposition ecology. Additionally, the processes and dynamics of these microbes may be applied in forensic science, particularly concerning estimating the postmortem interval (PMI) [4–6].

Recently, several studies have utilized culture-independent, high-throughput sequencing technologies and bioinformatic analysis to determine the postmortem microbial community composition associated with cadaver skin [1, 4, 7, 8], the oral cavity [7–9], and the intestinal tract [1, 4, 7, 9–11]. Many of these studies have mainly focused on microbial succession within the long-term decomposition process [1, 5, 6, 12] rather than the immediate change after death when there is no obvious putrefaction of the corpse [13]. These studies mainly collected samples from body sites that have indigenous microbes, such as the skin, intestine, and oral cavity. Postmortem microbial succession in internal organs, which are presumed to be sterile, has rarely been reported. It is important to study microorganisms of internal organs associated with corpse decomposition, because the presence/absence and the abundance of certain bacteria may indicate early PMI (EPMI). Compared to a long PMI (LPMI), the EPMI estimation is more significant in forensic practice, as it improves the efficiency of case detection [14–16].

Studies have indicated a rapid microbial succession [17] from aerobic bacteria to anaerobic bacteria [18] in early decomposition of most body sites. In addition to changes in the microbial communities of specific locations within the body, bacteria can transmigrate from one organ to adjacent organs locally after death, or to distant locations via vascular channels or some unknown mechanisms [13]. Burcham et al found significant increases in relative abundance of *Clostridium* in the brain, heart, spleen, and liver samples, as the exudation of body fluids during long-term decomposition [2]. Their study also demonstrated that gene transcripts of multiple metabolic pathways were abundant in these organs, and the transcripts associated with the stress response and dormancy increased during the decomposition[2]. Some studies have utilized intranasal inoculation of *Staphylococcus aureus* and *Clostridium perfringens* to investigate their postmortem structure and functional dynamics [14]. In heart, liver, spleen, kidney and other parenchymal organs, the detection rate of *S. aureus KUB7* displayed undulating positivity over time. For example, *S. aureus KUB7* was positive in the kidneys at 1 hour postmortem. However, there is limited information about the early changes in the postmortem microbial communities in mammalian animals, especially about the microbiome of extraintestinal locations [15, 16]. Thus, systematic studies are needed to investigate postmortem microbial communities changes of internal organs in healthy individuals to provide basic data. In the current study, we characterized and compared the microbial composition of postmortem internal organs (brain, heart, liver, and kidney). In addition, we characterized the shift in microbial assemblages through the EPMI in a mouse decomposition model. Understanding the shifts in microbial community composition and functional-associated pathway levels may be beneficial to studies in decomposition ecology, forensic science, and even organ transplantation.

Results

1. Microbial variation in internal organs after death

1.1 Relative abundance profiles of the microbial community during 1 day of decomposition

120 organ samples, including those from the brain, heart, liver, and kidneys, were collected from 30 mouse remains of 5 timepoints over 1 day of decomposition during 1 day of decomposition. In our study, no valid bacterial sequences were detected in the negative controls, indicating that the sequencing data are reliable. To analyze microbial community succession in every organ, the microbial community composition profiles in the four organs were described separately.

In the brain samples, at the genus level (Fig. 1A and Fig. S1A), *Ochrobactrum* (10.37%~18.54%) and *Sediminibacterium* (3.23%~17.74%) were dominant and showed a similar decreasing relative abundance profile along PMI progression. *Acinetobacter*, *Cupriavidus*, and *Agrobacterium* showed increasing abundance profiles. In particular, the relative abundance of *Agrobacterium* significantly increased (11.99% ± 0.41%) at 8 hours compared with 0.5 hours (4.32% ± 0.28%, $P = 0.004$) and 4 hours (4.02% ± 0.79%, $P = 0.004$) ($P < 0.01$, KW-test, Fig. 2A). At the phylum level (Fig. S2A), Proteobacteria (54.06%~87.80%) was the most prevalent in all brain samples. The relative abundance of Bacteroidetes was higher in the H0.5Brain (19.31%±0.81%) and H4Brain (19.63%±3.27%) samples than in the samples from the other three groups (the P values of the six paired comparison groups were all 0.000, $P<0.001$, LSD t- test). Proteobacteria showed different succession structures during decomposition. In addition, the relative abundances of Cyanobacteria and Thermi illustrated an increase during 12 hours of decomposition. At the order level (Fig. S2A), Rhizobiales (21.97%~31.65%) was dominant in all brain samples. The relative abundances of Saprospirales, Caulobacterales, and Thermales decreased, while those of Burkholderiales and Pseudomonadales showed increasing profiles during 1 day of decomposition. At the species level (Fig. S2A), the relative abundance of *Bifidobacterium longum* showed a peak value at hour 4 after death. *Acinetobacter johnsonii* showed a peak value at hour 12 after death. The abundances of *Deinococcus geothermalis* and *Sphingomonas azotifigens* abundances increased during decomposition.

In the heart samples, at the genus level (Fig. 1B and Fig. S1B), *Thermus* (14.52%~25.12%) was more abundant than the other genera in all the heart sample groups. The relative abundances of *Enhydrobacter*, *Caulobacter*, and *Methyloversatilis* gradually decreased during 1 day of decomposition. However, the relative abundance of *Pseudomonas* increased to 11.38% at 8 hours after death. The relative abundances of *Sphingomonas* and *Cupriavidus* increased to peak values of 7.93% and 12.58%, respectively, at 12 hours after death. At the phylum level (Fig. S2), Proteobacteria (47.49%~67.28%) and Thermi (16.70%~27.90%) were dominant in the early postmortem heart samples. The relative abundance of Firmicutes gradually increased during 1 day of decomposition, while that of Actinobacteria decreased. At the order level (Fig. S2B), Pseudomonadales (15.21%~27.57%), Thermales (14.52%~25.12%), and Burkholderiales(15.41%~20.26%) were dominant in all heart samples. The relative abundance of Sphingomonadales increased to a peak value of 8.96% at 12 hours after death. Rhizobiales showed a gradual increasing abundance profile during 1 day of decomposition. Furthermore, the relative abundance of Deinococcales increased to 4.72% at 12 hours after death. However, the relative abundance of Rhodocyclales, Rhodospirillales, and Caulobacterales decreased during 1 day of decomposition. At the

species level (Fig. S2B), *Pseudomonas viridiflava*, *Sphingomonas azotifigens*, and *Deinococcus geothermalis* were dominant in all the postmortem heart samples.

In the liver samples, at the genus level (Fig. 1C and Fig. S1C), *Thermus* (16.83%~24.22%) and *Cupriavidus* (11.40%~14.35) were dominant in all the postmortem liver sample groups. The relative abundance of *Microbacterium* gradually decreased to zero percent at 24 hours after death. In contrast, the relative abundances of *Acinetobacter*, *Cupriavidus*, and *Pseudomonas* gradually increased during decomposition. The genera *Paracoccus* and *Cryocola* were detected only half an hour after death. *Prevotella* showed a significant increase in relative abundance at 4 hours (1.14% ± 0.57%) compared with that at 0.5 hours (0.44% ± 0.38%) (P=0.037, P < 0.05, KW-test, Fig. 2B). At the phylum level (Fig. S2C), Proteobacteria (48.29%~62.36%) and Thermi (18.79%~25.39%) were dominant in all the liver sample groups. Actinobacteria, Firmicutes, Bacteroidetes, and Cyanobacteria showed relative abundances of more than 1% in all the liver sample groups. Among these phyla, Actinobacteria gradually decreased in relative abundance during 1 day of decomposition. At the order level (Fig. S2C), Burkholderiales (15.25%~20.72%), Pseudomonadales (14.59%~27.66%), and Thermales (16.83%~24.22%) were dominant in all the liver sample groups. The relative abundance of Clostridiales gradually increased during 1 day of decomposition, while that of Actinomycetales decreased during decomposition. Rhodobacterales immediately decreased in relative abundance before 4 hours after death. At the species level (Fig. S2C), *Pseudomonas viridiflava*, *Sphingomonas azotifigens*, and *Sphingomonas azotifigens* were dominant in all the liver sample groups. *Paracoccus marcusii* decreased in relative abundance before 4 hours after death.

In the kidney samples, at the genus level (Fig. 1D and Fig. S1D), *Thermus* (7.40%~31.59%) was dominant. The relative abundances of *Acinetobacter* and *Pseudomonas* increased during 8 hours of decomposition. The relative abundance of *Methyloversatilis* decreased during 1 day of decomposition. *Bacillus* was significantly increased at 4 hours compared with 0.5 hours (P=0.045, P <0.05, KW-test, Fig. 2C). *Turicibacter* exhibited a significantly higher relative abundance in the H24Kidney group (1.33% ± 0.51%) than in the other kidney sample groups (v.s. H0.5; P = 0.038; v.s. H4, P=0.031; v.s. H8, P=0.013; v.s. H12, P=0.021, P <0.05, KW-test, Fig. 2D). At the phylum level (Fig. S2D), Proteobacteria (41.37%~60.51%), Thermi (8.00%~32.14%), and Firmicutes (7.35%~10.79%) were dominant in all the postmortem kidney sample groups. The relative abundances of Fusobacteria and Cyanobacteria gradually decreased during 1 day of decomposition, while those of Proteobacteria and Actinobacteria gradually increased during decomposition. At the order level (Fig. S2D), Pseudomonadales (11.94%~22.23%) and Thermales (7.40%~31.59%) were dominant orders in all the kidney sample groups. During 1 day of decomposition, the relative abundances of Streptophyta, Clostridiales, and Rhodocyclales gradually decreased. However, the abundances of Burkholderiales, Rhizobiales, Bacteroidales, and Actinomycetales gradually increased during this decomposition period. At the species level (Fig. S2D), *Paracoccus marcusii* and *Lactobacillus reuteri* had an increasing abundance profile across the 12 hours after death.

1.2 Comparison of alpha and beta diversity at different timepoints

Alpha diversity was measured by the Shannon index, Pielou's evenness, Good's coverage index, observed species index, Faith's PD index, and Chao1 index in this work. Samples in the H8Brain and H24Brain groups had significantly lower alpha diversity (measured as Shannon diversity, H8 v.s. H0.5, P=0.035; H24 v.s. H0.5, P=0.003 (Fig. 4A), Pielou's evenness, H8 v.s. H0.5, P=0.009; H24 v.s. H0.5, P=0.046 (Fig. S3A), and Good' s coverage index H8 v.s. H0.5, P=0.028; H24 v.s. H0.5, P=0.035 (Fig. S3C)) than those in the H0.5Brain group (P<0.05, KW-test). Faith's PD index, indicating the phylogenetic distances of OTUs in a sample, had a significantly lower value in the H0.5Brain group than in the H8Brain (P=0.0015), H12Brain (P=0.014), and H24Brain (P=0.0024) groups (P<0.05, LSD t-test, Fig. S3B).
Faith's PD index was significantly lower in the H24Liver group than in the H4Liver (P=0.009) and H8Liver (P=0.003) groups (P<0.01, Dunnett T3 test, Fig. S3D). According to a comparison of alpha diversity in the kidney groups, the observed species index demonstrated a significantly lower value in the H12Kidney group than in the H4Kidney (P=0.01) and H8Kidney (P=0.000) groups (P < 0.01, Dunnett T3 test, Fig. S3E). The samples in the H12Kidney group showed a significantly lower value of Chao 1 index than those in the H4Kidney (P=0.01) and H8Kidney (P=0.000) groups (P < 0.01, Dunnett T3 test, Fig. S3F).

To visualize the similarities and dissimilarities in community composition between samples, as a measure of beta diversity, PCoA plots were calculated based on the weighted UniFrac dissimilarity index. Overall, PCoA of brain samples revealed two distinct clusters (the PCoA explained 42.8% of the variation): one including samples of the H0.5Brain and H4Brain groups and another including samples from the H8Brain, H12Brain, and H24Brain groups (Fig. 3E). PCoA of kidney samples showed three clusters: a cluster of samples from the H0.5Kidney, H4Kidney, and H8Kidney groups; a cluster of samples from the H12Kidney group; and a cluster of samples from the H24Kidney group (Fig. 3H). Liver and heart samples did not show significant clusters according to beta diversity analysis (Fig. 3).

To identify the taxonomic bacteria with significantly different abundances among different PMIs for internal organs, the LEfSe method was used for biomarker analysis (Fig. 4). As shown in Fig. 4A, *Sediminibacterium* and *Ochrobactrum* were representative genera in the H0.5Brain group. *Lactobacillales*, and *Mycoplana* were significant microbes in the H4Brain group. *Agrobacterium* was the significant genus in the H8Brain group. *Deinococcus* and *Acinetobacter*, were representative microbes in the H12Brain group. *Cupriavidus* and *Cryocola* were representative microbes in the H24Brain group.

When the taxonomic composition was compared within different decomposition stages in the heart (Fig. 4B), *Phascolarctobacterium*, *Xanthomonadaceae*, *Sphingobium*, and *Ellin6529* were significant microbes in the H0.5Heart group; *Enterobacteriaceae*, *Lysinibacillus*, and *Steroidobacter* were detected as representatives in the H4Heart group; Proteobacteria was significant in the H8Heart group; *Cupriavidus* was regarded as a significant microbe in the H12Heart group; and *Lactococcus* showed significance in the H24Heart group. In regard to the liver groups, Microbacteriaceae,Comamonadaceae, and *Caulobacter* were significant microbes in the H0.5Liver group (Fig. 4C); Actinomycetales, PRR_12, and Solibacterales were representative microbes in the H4Liver group; *Myroides*, *Kocuria*, *Citrobacter*, and Streptomycetaceae were significant microbes in the H8Liver group; Gemmatimonadetes and *Raphanus* were representatives

in the H12Liver group; and *mitochondria* were regarded as significant microbes in the H24Liver group. For the kidney groups (Fig. 4D), Enterobacteriaceae and Streptophyta were significant microbes in the H0.5Kidney group; *Limnobacter*, Sphingomonadaceae, Clostridiales, Sphingomonadaceae, Hyphomonadaceae, and Planococcaceae were significant in the H4Kidney group; *Thermus*, Bacteriovoracaceae, and *Luteimonas* were significant in the H8Kidney group; Rhodobacterales, *Perlucidibaca*, Bacillales, *Flavobacterium*, *Anoxybacillus*, *Comamonas*, and Rhodospirillaceaewere significant in the H12Kidney group; and *S24_7*, Oxalobacteraceae, *Turicibacter*, *Bacteroides*, *Akkermansia*, *Cupriavidus*, and Deltaproteobacteria were significant microbes in the H24Kidney group.

2. Differential postmortem microbial community structure and diversity between different organs

Alpha diversity was significantly different between the brain and the other organs (heart, kidney, and liver) ($P < 0.05$, Student's t-test (LSD), KW-test, Fig. 5). The brain groups exhibited lower observed amplicon sequence variant (ASV) richness values than the other organs at half an hour, 4 hours, 8 hours, and 24 hours after death. Kidney samples showed the lowest observed ASV richness values among the other organ groups at 12 hours after death (Fig. 5). Beta diversity based on weighted UniFrac distance showed obvious clustering at the early decomposition stage according to the organ, while the distinction decreased with the decomposition process (Fig. 5). In general, the brain samples were dominated by the bacterial genera *Acinetobacter*, *Cupriavidus*, *Ochrobactrum*, and Sediminibacterium, while the other organs were dominated by *Thermus*, *Enhydrobacter,* and *Pseudomonas* (Fig. 1).

LEfSe analyses were applied to detect representative microbes among the different sample sites during decomposition at different taxonomic levels (Fig. 6). The number of significant taxa in each organ increased before 8 hours and decreased from then on, leading to no significantly differentially abundant taxa in any organ at 24 hours after death, with a linear discriminant analysis (LDA) threshold of 4 (Fig. 6). Half an hour after death (Fig. 6A), *Agrobacterium*, *Sediminibacterium*, and *Ochrobactrum* were detected as significantly differentially abundant genera in the H0.5Brain group; Comamonadaceae, *Sphingomonas,* and *Sphingomonas azotifigens* were detected in the H0.5Heart group at multiple levels; *Pseudomonas*, *Cupriavidus*, *Deinococcus*, and *Cryocola* were significantly differentially abundant genera in the H0.5Liver group; *Pseudomonas viridiflava* and *Deinococcus geothermalis* were detected as significantly differentially abundant species in the H0.5Liver group; and *Enterobacteriaceae*, Streptophyta and *Methyloversatilis* were significantly differentially abundant bacteria in the H0.5Kidney group. After 4 hours of decomposition (Fig. 6B), Bradyrhizobiaceae and *Agrobacterium* were significantly differentially abundant microbes in the H4Brain group; *Pseudomonas*, *Acinetobacter,* and *Sphingomonas* were detected as representative genera in the H4Heart group. In addition, *Sphingomonas azotifigens*, *Pseudomonas viridiflava,* and *Deinococcus geothermalis* were significantly differentially abundant species in the H4Heart group. *Thermus*, *Limnobacter*, *Perlucidibaca*, *Methyloversatilis,* and *Flavobacterium* were significantly differentially abundant genera in the H4Kidney group. *Moraxellaceae* and *Cupriavidus* were detected as significantly differentially abundant microbes in the H4Liver group. After 8 hours of decomposition (Fig. 6C), *Cupriavidus*, *Ochrobactrum*, *Agrobacterium*, *Sediminibacterium,* and *Acinetobacter* were significantly differentially abundant genera in the H8Brain group; *Sphingomonas*,

Pseudomonas, and *Deinococcus* were significantly differentially abundant genera in the H8Heart group. *Pseudomonas viridiflava*, *Sphingomonas azotifigens,* and *Deinococcus geothermalis* were significantly differentially abundant species in the H8Heart group. In the H8Kidney group, *Thermus* and *Methylobacterium* were significantly differentially abundant genera. After 12 hours of decomposition (Fig. 6D), *Acinetobacter*, *Cupriavidus*, *Acinetobacter,* and *Agrobacterium* were detected as significantly differentially abundant genera in the H12Brain group; *Thermus*, *Pseudomonas*, *Sphingomonas,* and *Pseudomonas* were representative genera in the H12Heart group. *Sphingomonas azotifigens* and *Pseudomonas viridiflava* were detected as significantly differentially abundant species in the H12Heart group. *Perlucidibaca* and *Flavobacterium* were significantly differentially abundant genera in the H12Kidney group. We also counted the genera with continuous difference in the comparison of four organs based on the LDA effect size (LEfSe) analysis results (Table 1).

3. Metabolically active members in postmortem organs during decomposition

The metabolic pathways based on the KEGG database were used to link microbial genomic information by the PICRUSt2 algorithm with higher-order functions that were significantly altered during 1-day decomposition. To facilitate writing, the organ groups harvested before 4 hours after death were called “before 4 h”, while those harvested after 4 hours of decomposition were called as “after 4 h”. Broad classes of metabolic pathways within the samples are presented in Fig. 7. The enriched pathways of the current study were amino acid metabolism, carbohydrate metabolism, cofactor and vitamin metabolism, xenobiotic biodegradation and metabolism, other amino acid metabolism, terpenoid and polyketide metabolism, lipid metabolism, and energy metabolism, which are summarized in Fig. 7A. The top 5 relative abundance pathways were similar in the four organs. Certain pathways, including ketone body synthesis and degradation; ansamycin biosynthesis; valine, leucine, and isoleucine biosynthesis; C5-branched dibasic acid metabolism; and fatty acid biosynthesis, were dramatically enriched in “after 4 h” samples, compared to “before 4 h” samples of the brains and hearts (Fig. S4, $P < 0.05$, KW-test). A heatmap shows particular pathways that were differentially abundant according to the organ (Fig. 7B). According to comparisons of different organs at 0.5 hours, selenocompound metabolism, histidine metabolism, and several amino acid metabolism pathways were obviously more enriched in the brain than in the other organs. The bacterial chemotaxis and flagellar assembly pathways were depleted in kidney samples. After 4 hours of decomposition, pantothenate and CoA biosynthesis, selenocompound metabolism, and amino acid metabolism were enriched in the H4Brain group compared with in the other organ groups. After 8 hours of decomposition, the biotin, lipoic acid metabolism, carbon fixation in prokaryotes and terpenoid backbone biosynthesis pathways were depleted in brain samples compared to those in samples from the other organs. After 12 hours of decomposition, the pyruvate metabolism pathway was enriched in the kidney compared with in the other organs.

Discussion

The common thanatomicrobiome sampling method in previous studies was continuous swabbing in the same bodies. Different individuals were sampled each time, rather than repeatedly sampling the same bodies, with the purpose of preventing exposure of internal organs to surrounding environment and leading to potential microbiota related changes. Through 16S rRNA MiSeq sequencing, we directly investigated the temporal dynamics of microbial community composition and predicted gene function within cadavers. As posited, the microbial abundance and composition appeared to notably shift along with PMI timepoints in different organs. The differences were most striking in the brain (Fig. 3 and Fig. S3). *Acinetobacter* immediately increased in abundance at hour 8 in brain samples (Fig. S1), which is an aerobic, nonfermentative, gram-negative pathogenic bacilli and previous reported in a swine carcass using fluorescence in situ hybridization (FISH) [19]. *Cupriavidus* and *Agrobacterium* were increased after 8 hours of decomposition in brain samples. A previous study reported the decomposition ability of *Cupriavidus basilens* in organic matter since it accelerates organic phosphate decomposition, which could acidify microbial cells and cause the release of orthophosphate from mineral phosphate [20]. At the phylum level, *Bacteroidetes* and *Proteobacteria* showed different succession structures during decomposition, which could be important information in PMI estimation. The phyla *Proteobacteria* and *Bacteroidetes* are reported participate in organic matter degradation and in carbon turnover [21]. At the species level, *Bifidobacterium longum* has a peak relative abundance at hour 4 and is considered to be a scavenger, possessing multiple catabolic pathways to scavenge a large variety of nutrients from extracellular polymers. [22]. The relative abundance of *Deinococcus geothermalis* increased, which can combat oxidative stress caused by aerobic lifestyle and by oxidative biocides, suggesting that exacting this species from corpses may facilitate in industrial usage. [23]. *Sphingomonas azotifigens*, a nitrogen-fixing bacterium [24], also increased in abundance during decomposition.

When analyzing microbial succession of internal organs during decomposition, we observed some interesting findings. The microbial composition of brain samples shifted from facultative anaerobes to obligate aerobes, while that of heart samples shifted from obligate aerobes to facultative anaerobes (Fig. 4). *Proteobacteria* and *Cupriavidus* were differentially abundant in the H8Heart and H12Heart groups, which was similarly observed in the brain sample groups. In the heart samples, *Enhydrobacter* and *Caulobacter*, belonging to Alphaproteobacteria, showed a decreasing abundance profile. *Caulobacter* uses energy-dependent proteases to control protein destruction in a highly specific manner [25]. *Methyloversatilis* and *Sphingomonas* are reportedly decomposers that have been isolated from various environments and were also detected in postmortem heart samples in this work [26]. In the liver groups, *Microbacterium*, which gradually disappeared with body degradation and includes aerobiotic bacteria that utilize riboflavin (vitamin B2) as a carbon source [27], was identified and has been reported previously in murine decomposition[28]. *Paracoccus* and *Cryocola* were observed in the H0.5Liver group. *Paracoccus* is a biochemically versatile genus possessing a variety of metabolic pathways through which a wide range of diverse compounds can be degraded. *Cryocola* was found in the co-composting of organic wastes [29]. Comamonadaceae, a family of *Betaproteobacteria*, was also significantly enriched in the H0.5Liver group, meaning that nutrition of the liver was sufficient at the beginning of death. With oxygen consumption, Actinomycetales, gram-positive and anaerobic bacteria, were dominant in the

H4Liver group. This order can be found mostly in soil and decaying organic matter. We detected *Rickettsiales* as a representative the H24Liver group. All bacteria of this order are short coccobacillary organisms, strictly intracellular bacteria and thus need to survive in animal host. This result surprised us since, even though the body did not encounter arthropods, the microbial community could provide some important information on the appearance of arthropods. The representative microbes shift from facultative anaerobes, such as Enterobacteriaceae, to aerobic bacteria (*Limnobacter*, *Deinococcus*, and Rhodobacterales), and then to obligate anaerobes, such as *Bacteroides*, in H24Kidney group (Fig. 4D). *Leptothrix*, observed in the H24Kidney group, is a sheathed filamentous bacterium that can generally be found in environments with sufficient organic matter. The relative abundance of *Turicibacter*, which has most commonly been found in the gut of animals, showed a significant increase in the H24 group compared with the other kidney sample groups (Fig. 2D). Meanwhile, *Lactobacillus reuteri*, one of the most ubiquitous species of mammalian gut microbes, had an increasing abundance profile during 12 hours of decomposition in the kidney samples. These results suggested the possibility of gut microbes participating in body decomposition after death.

Microbial alpha diversity showed a slightly fluctuating decrease during 1 day of decomposition, as was observed previously for bacterial alpha diversity in human [1], porcine [8], and murine [5] remains. This study demonstrated that the microbial community evenness of the H0.5Brain group was higher than that of the other brain sample groups according to a higher Pielou's evenness value. Faith's PD index comparison among the brain sample groups indicated that the microbial species affinity in postmortem organs decreased with time. Additionally, the decline in Good's coverage index showed that the proportion of species detected decreased with brain decomposition. The alpha diversity change trends in other organs were not as obvious as those in the brain groups. We supposed that the incongruence of decay stages among different organs occurred mainly because of their microbial composition at the moment of death. The brain samples formed two clusters in a PCoA plot based on weighted UniFrac distance according to the decomposition stage. In addition, the groups separated in the PCo1 direction that explained 42.8% of the variance, which was higher than that for the PCoA of the other organs. These results all illustrated obvious microbial composition succession in postmortem brain samples. We also detected some marked pathways predicted to be associated with metabolism that were enriched in our samples, including lipid metabolism, terpenoid and polyketide metabolism, amino acid metabolism, and carbohydrate metabolism (Fig. S4). The significant increase in the relative abundance of these pathways suggested that organic synthesis and degradation processes were present after 8 hours of decomposition. This result explained the increase in the relative abundances of some microbes during decomposition. These findings provide future research directions for the related analysis of microbial communities and metabolic pathways.

Importantly, postmortem microbiota changes are organ specific [30]. Specifically, the microbial composition in postmortem organs (Fig. 1) differed. *Acinetobacter*, *Cupriavidus*, and *Ochrobactrum*, dominant in postmortem brain samples, are environmental organisms, especially in soil, and are considered opportunistic pathogens in humans in the hospital. *Enhydrobacter* is reportedly a member of the mammalian intestinal microbiome and was dominant in postmortem kidney and liver samples. The

possible reason may be that the locations of the liver and kidney are near the intestine of the body. *Thermus*, dominant in the heart, liver, and kidney samples, was found in the human corpses [31]. Based on the comparison of alpha diversity, a lower observed ASV value was observed in the brain than in the other organs ($P < 0.05$, Fig. 5), which suggested that postmortem microbial diversity depends on the distance between the organ and the gut. The kidney and liver, located close to the gut, begin to putrefy in a specific natural order at the early stage of decomposition [30]. PCoA based on the beta diversity index showed a tendency to separate all the organ groups at the very beginning of decomposition, while the tendency was not clear over time (Fig. 5). Likewise, LEfSe analysis demonstrated that no difference remained after 1 day of decomposition (Fig. 6). All of the results confirmed that the compositions of the microbes participating in organ degradation became much more similar over time [32]. To further detected significant microbes of different organs, we summarized the continuous significant genera in different organ based on the P-value and LDA score of LEfSe analysis (Table 1). *Ochrobactrum*, *Agrobacterium*, *Leptothrix*, *Aminobacter*, *Bradyrhizobium*, and *Phyllobacterium* had significant higher relative abundances in postmortem brain samples than in other organs during 1 day of decomposition. *Ochrobactrum* [33] and *Agrobacterium* [34] were reported to be associated with corpse decomposition. *Leptothrix* can be found in environments with sufficient amounts of organic matter, which may suggest its decomposition capacity. *Bradyrhizobium* has been reported to have the capacity to oxidize sulfur [35], carry out denitrification, and fix nitrogen. *Phyllobacterium* was reported to exhibit obvious changes in postmortem oral microbiota community [36], which may suggest that it invades the brain from the mouth after death. *Sphingomonas* was found to be a continuously continuous significant genus of heart compared to other organs, and was also reported in internal organs of human corpses [30]. This genus is considered to comprise ammonia-oxidizing bacteria that can decompose polycyclic aromatic hydrocarbons positive for nitrogenase [37]. In addition, it has been reported produce NH_3 using pig carcass proteins as a substrate [38]. We identified *Lysinibacillus* and *Perlucidibaca* as significant differential genera in kidney compared to other organs, and these genera have been reported in other decomposition studies [39].

The differences among organs lie not only in the microbial composition but also in the relative abundance of some metabolic active pathways. Selenium is widely distributed throughout the body, especially in the brain, even under dietary selenium deficiency. When the body dies, selenocompounds in the brain degrade, as the relative abundance of selenocompound metabolism was higher in the H0.5Brain group than in the other organ groups [40]. The histidine metabolism pathway was activated in the H0.5Brain group but not in other organs. Histamine in the brain is a neurotransmitter formed by the decarboxylation of histidine and regulates diverse physiological functions. Histamine N-methyltransferase (HNMT) is a histamine-metabolizing enzyme expressed in the brain. These results all explained the differential abundance of pathways among different organs [41]. Several amino acid metabolism pathways, including those for D-alanine, glycine, serine, and threonine metabolism, were activated in the brain compared to those of the other organs, possibly because the protein content is highest in the brain. In the H0.5Kidney samples, the relative abundances of the genes associated with the bacterial chemotaxis and flagellar assembly pathways were lower than those in the other organs. This

result means that microbial chemotactic activity was not active in kidney samples immediately after death because chemicals such as nutrients and toxins were not yet released [42]. After 4 hours of decomposition, the microbial behaviour was continually active in brain samples. The relative abundances of the pantothenate and CoA biosynthesis, selenocompound metabolism, and amino acid metabolism pathways were higher in the H4Brain group than in the other organ groups. In some bacteria, the production of phosphopantothenate by pantothenate kinase is the rate limiting and most regulated step in the biosynthetic pathway [43]. Similar to those in the H0.5Brain group, some amino acid metabolism pathways, such as those for glycine, serine, threonine, histidine, alanine, aspartate, glutamate, and lysine, were activated because of some bacterial behaviour. For example, the lysine biosynthetic pathway is closely associated with bacterial activity. Two products of this pathway, lysine and mesodiaminopimelate (m-DAP), are directly involved in bacterial cell wall synthesis [44]. After 8 hours of decomposition, biotin, lipoic acid metabolism, carbon fixation pathways in prokaryotes and the terpenoid backbone biosynthesis pathway were inhibited in brain samples compared to the other organ samples. Biotin is a water-soluble vitamin that functions as a cofactor of enzymes involved in carboxylation reactions to maintain metabolic homeostasis [45]. Lipoic acid, an enzyme cofactor, is related to lipoylation strategies of microbial pathogens, which can affect pathogenesis and virulence [46]. The lipoic acid metabolism, relatively activated in heart, liver and kidney, may suggest the proliferation of pathogens in these organs. Cyanobacteria, a group of phototrophic bacteria, use light as energy to generate phosphate bond energy (ATP) and reduce agents [such as NAD(P)H and reduced ferredoxin] by photosynthetic electron transport [47]. Thus, the inhibition of carbon fixation pathways in the brain may be associated with the decrease in the relative abundance of Cyanobacteria. After 12 hours of decomposition, pyruvate metabolism pathway was enriched in the kidney compared with the other organs. Lactic acid bacteria can produce pyruvate and lactate by use of carbohydrates, organic acids, and amino acids. The LEfSe analysis results also revealed *Lactobacillales* as a significant bacterium in H12Kidney samples in contrast to in the other organs at 12 hours. This study described and compared the microbial community composition among different organs in a 1-day decomposing cadaver in detail. The functional prediction of the microbial community in the early decomposition body was also analyzed in this work. This work provided basic information on the microbial composition of internal organs immediately after death, which may facilitate organ transplantation.

However, there are still some limitations in this study. To give a basic look at the microbial community succession of internal organs during decomposition, we chose a controlled-environment chamber to place remains. A lot of factors interfered with the body decomposition in a real case, such as humidity, temperature, and insect behavior. Based on the results of the current study, the influence of outside environment and complex inter-reaction with the hosts should be studied in the future. Besides, the sample size of this study was limited, which may make the results of statistical analysis less conclusive. Future large-scale studies investigating human remains decomposition in mortality events will expand the results of this work.

Conclusion

In conclusion, postmortem internal organs contained bacteria from 0.5 hours to 24 hours after death but had a relatively low species richness and abundance of bacteria. Interestingly, the microbiome changed after death, and more importantly, these alterations were organ specific. The dominant microbes differed from one organ to another, while they tended to become more similar over time. Substantial differences in the microbial relative change rate between different organs over time due to the initial microbial composition differed. The thanatomicrobiome variation by body site provides new knowledge into decomposition ecology. These findings may also be valuable in early PMI estimation and organ transplantation.

Methods

Sample collection protocol

Adult male C57BL/6J mice (18-25 g, 6-10 weeks, n = 30) were acquired from the Experimental Animal Center of Xi'an Jiaotong University and cohoused under standard lighting (light/dark periods of 12 hours), temperature (25.0 ± 1.5°C), and relative humidity (50.0 ±7.0%) conditions at the animal centre of Xian Jiaotong University. They were housed and handled daily under laboratory conditions for at least 7 days prior to the start of study. Water and food were available *ad libitum*. All animal experiments were approved by institutional animal care and use committee of Xi'an Jiaotong University (IRB: 2017-388). The experiment was performed under the same conditions of light, temperature, and relative humidity described above. Mice were euthanized by isoflurane inhalation followed by cervical dislocation. After cervical dislocation, mice were placed in a controlled-environment chamber (PRX-350D, ZuoLe, ShangHai) with constant temperature (Ta, 25±1.5℃) and relative humidity (RH, 50±7%) at Xi'an Jiaotong University, College of Forensic Medicine. Internal organic samples (brain, heart, liver, and kidneys) were harvested from mouse corpses following aseptic principles at half an hour, 4 hours, 8 hours, 12 hours, and 1 day (6 mice per timepoint at random). Concretely, every surgical instrument was autoclaved before used. The clean bench was sterilized under ultraviolet light for at least 2 hours before operation. Operators wore sterile surgical clothes during operation. In addition, we swabbed surgical instruments with sterile swabs and set them as negative controls. 120 samples were then immediately stored at −80°C until further experimentation.

Postmortem microbiota analysis by 16S rRNA gene sequencing

Total genomic DNA was extracted from samples by OMEGA Soil DNA Kit (D5625-01) (Omega Bio-Tek, Norcross, GA, USA) according to the manufacturer's recommendations. The quantity and quality of extracted DNA were evaluated by NanoDrop ND-1000 spectrophotometer (Thermo Fisher Scientific, Waltham, MA, USA) and agarose gel electrophoresis. The microbial 16S rRNA gene V3 and V4 regions were amplified by polymerase chain reaction (PCR) with the universal primers 338F (5'-ACTCCTACGGGAGCAGCAGCA-3') and 806R (5'-GGACTACVSGTATCTAAT-3'). The PCR components consisted of 5 μl of buffer (5×), 0.25 μl of DNA Polymerase (5 U/μl), 2 μl (2.5 mM) of dNTPs, 1 μl (10 μM) of 338F and 806R primer, 1 μl of DNA template, and 14.75 μl of ddH_2O. The PCR cycling included an

initial denaturation for 30 s at 98°C, 30 cycles annealing of 15 s at 98°C, 30 s at 50°C, and 30 s at 72°C, and an extension for 5 min at 72°C. PCR products were purified with Vazyme VAHTSTM DNA Clean Beads (Vazyme, Nanjing, China). quantified by a Quant-iT PicoGreen dsDNA Assay Kit (Invitrogen, Carlsbad, CA, USA). Equal amount of amplicons were paired-end 2×250 bp sequenced on the Illumina MiSeq platform with a MiSeq Reagent Kit v3 at Shanghai Personal Biotechnology Co., Ltd. (Shanghai, China).

Sequence bioinformatics analysis

Microbiome bioinformatic analysis was performed on QIIME2 platform [48] following the official tutorials (https://docs.qiime2.org/2019.4/tutorials/), with slight modification. In brief, we demultiplex the raw sequence data using the demux plugin followed by primer trimming with the cutadapt plugin [49]. The sequence data were then quality filtered, denoised, merged, and cleaned from chimeric reads using the DADA2 plugin [50]. Nonsingleton amplicon sequence variants (ASVs) were aligned with mafft [51] and used to construct a phylogeny with fasttree2 [52]. The richness and evenness of ASVs among samples were compared by generating ASV-level ranked abundance curves. The classify-sklearn naïve Bayes taxonomy classifier [53] plugin with the SILVA Release 132 Database was used to assign taxonomy to the ASVs. 16S rRNA gene sequence data analyses were mainly performed with QIIME2 and R packages (v3.2.0). Alpha diversity metrics included Chao1 [54], observed species, Shannon [55], Simpson [56], Faith's phylogenetic diversity (PD) [57], Pielou's evenness [58] and Good's coverage [59]. Beta diversity metrics included Jaccard metrics, Bray-Curtis metrics, and UniFrac distance [60, 61]. To visualize the structural variation in microbial communities, we utilized principal coordinates analysis (PCoA), nonmetric multidimensional scaling (NMDS) and unweighted paired-group method with arithmetic means (UPGMA) hierarchical clustering [62]. Permutational multivariate analysis of variance (PERMANOVA) was applied to assess the significance of microbial community structure differentiation among groups [63]. The taxonomy compositions and abundances were visualized using MEGAN [64] and GraPhlAn [65]. Linear discriminant analysis (LDA) effect size (LEfSe) was performed to detect differentially abundant taxa as potential biomarkers across groups [66]. An LDA threshold score of 3 and a significant alpha of 0.05 were used to detect biomarkers. Phylogenetic Investigation of Communities by Reconstruction of Unobserved States 2 (PICRUSt2) was applied to predict functional information [67] with the Kyoto Encyclopedia of Genes and Genomes (KEGG) (https://www.kegg.jp/) databases.

Statistical analysis

To compare microbial succession differences in different organs, the relative abundances of ASVs were summed in every sample. Based on the microbial relative abundance data of the adjacent death timepoints of the same organ, the dataset for the relative change rate in this period was obtained; please see supplementary material 1 for the detailed calculation. We compared the rates of different organs within the same PMI period. The statistical analyses in this work were conducted using SPSS software (v18.0, Chicago, IL, USA). Statistical analyses used in this study were Student's t-test, least significant

difference (LSD), Kruskal-Wallis rank-sum test (KW-test), analysis of variance (ANOVA), and Dunnett's T3 test according to the applicable conditions. Student's t-test generated *P* value. * represents $P<0.05$ (confidence interval of 95%), and ** represents $P<0.1$ (confidence interval of 90%), *** represents $P<0.001$ (confidence interval of 99.9%). Statistical tests, sample size, and exact *P* value are indicated in relevant figure legends.

Abbreviations

PMI
postmortem interval
PCoAs
principal coordinate analyses
PERMANOVA
permutational analyses of variance
16S rRNA
16S ribosomal RNA
EPMI
early postmortem interval (within 1 day)
LPMI
long postmortem interval (greater than 1 day)
PCR
polymerase chain reaction
ASVs
nonsingleton amplicon sequence variants
Faith's PD
Faith's phylogenetic diversity
NMDS
non-metric multidimensional scaling
UPGMA
unweighted paired-group method with arithmetic means
ANOSIM
analysis of similarities
LEfSe
linear discriminant analysis effect size
PICRUSt2
phylogenetic investigation of communities by reconstruction of unobserved states 2
KEGG
Kyoto Encyclopedia of Genes and Genomes
LSD
least significant difference

KW-test
Kruskal-Wallis rank-sum test
ANOVA
analysis of variance
FISH
fluorescence in situ hybridization

Declarations

Ethics approval and consent to participate

This work used only dead animals that had been sacrificed as a byproduct of other research. Mice were euthanized humanely by isoflurane inhalation followed by cervical dislocation under approved approval IRB: 2017-388.

Consent for publication

Not applicable.

Availability of data and materials

All raw sequence data used for our analyses have been uploaded to the National Center for Biotechnology Information Sequence Read Archive (NCBI-SRA) under BioProject number PRJNA746418: www.ncbi.nlm.nih.gov/bioproject/PRJNA746418. Four supplementary figures are available with the online version of this article.

Competing interests

The authors declare no conflict of interest.

Funding

This work was supported by the Council of National Natural Science Foundation of China (No. 81730056) and the Key Research and Development Program of Shaanxi (2020SF-133). The funders or supporters had no role in the study design, data collection, and interpretation, decision to publish, or preparation of the manuscript.

Author contributions

RL conceived the study, collected the samples, analysed the data, and wrote the manuscript. QW analysed the data. KZ collected the samples. HL collected the samples. XW, SR, and HL investigated the study process. QS, SF, and ZW reviewed and edited the article. ZW acquired the financial support for the project. All authors edited the manuscript and approved the final draft.

Acknowledgments

The authors thank Shanghai Personal Biotechnology Co., Ltd (Shanghai, China) for insightful assistance with the DNA sequencing and bioinformatics analysis.

Authors information

Author name	E-mail address	Affiliation
Ruina Liu	liuruina@stu.xjtu.edu.cn	1
Kai Zhang	zkzjly@126.com	1
Huan Li	1154736255@qq.com	2
Qinru Sun	qinrusun@xjtu.edu.cn	1
Xin Wei	weixin@stu.xjtu.edu.cn	1
Huiyu Li	lihuiyu@stu.xjtu.edu.cn	1
Siruo Zhang	hardworkingzsr@126.com	3
Shuanliang Fan*	xafansl@xjtu.edu.cn	1
Zhenyuan Wang*	wzy218@xjtu.edu.cn	1

Affiliation

[1]College of Forensic Medicine, Xi’an Jiaotong University, Xi’an 710061, China

[2]Xi 'an Mental Health Center Hospital, Xi’an 710061, China

[3]Department of Clinical Laboratory, Shaanxi Provincial People’s Hospital, Xi’an, Shaanxi 710068, PR China

[4]Department of Microbiology and Immunology, School of Basic Medical Sciences, Xi’an Jiaotong University, Xi’an, Shaanxi 710061, PR China

References

1. Metcalf JL, Xu ZZ, Weiss S, Lax S, Van Treuren W, Hyde ER, Song SJ, Amir A, Larsen P, Sangwan N, et al. Microbial community assembly and metabolic function during mammalian corpse decomposition. Sci (New York NY). 2016;351(6269):158–62.
2. Burcham ZM, Pechal JL, Schmidt CJ, Bose JL, Rosch JW, Benbow ME, Jordan HR. Bacterial Community Succession, Transmigration, and Differential Gene Transcription in a Controlled Vertebrate Decomposition Model. Front Microbiol. 2019;10:745.

3. Pechal JL, Benbow ME. Microbial ecology of the salmon necrobiome: evidence salmon carrion decomposition influences aquatic and terrestrial insect microbiomes. Environ Microbiol. 2016;18(5):1511–22.
4. Metcalf JL, Parfrey LW, Gonzalez A, Lauber CL, Dan K, Ackermann G, Humphrey GC, Gebert MJ, Treuren WV, Berg-Lyons DJE. **A microbial clock provides an accurate estimate of the postmortem interval in a mouse model system**. 2013, 2(2):e01104.
5. Liu R, Gu Y, Shen M, Li H, Zhang K, Wang Q, Wei X, Zhang H, Wu D, Yu K, et al. Predicting postmortem interval based on microbial community sequences and machine learning algorithms. Environ Microbiol. 2020;22(6):2273–91.
6. Belk A, Xu ZZ, Carter DO, Lynne A, Bucheli S, Knight R, Metcalf JL. **Microbiome Data Accurately Predicts the Postmortem Interval Using Random Forest Regression Models**. Genes (Basel) 2018, 9(2).
7. Hyde ER, Haarmann DP, Petrosino JF, Lynne AM, Bucheli SRJIJoLM. **Initial insights into bacterial succession during human decomposition**. 2015, 129(3):661–671.
8. Pechal JL, Crippen TL, Benbow ME, Tarone AM, Dowd S, Tomberlin JKJIJoLM. **The potential use of bacterial community succession in forensics as described by high throughput metagenomic sequencing**. 2014, 128(1):193–205.
9. Pechal JL, Schmidt CJ, Jordan HR, Benbow MEJSR: **A large-scale survey of the postmortem human microbiome, and its potential to provide insight into the living health condition**. 2018, **8**(1):5724.
10. Hauther KA, Cobaugh KL, Lee Meadows J, Sparer TE, Debruyn JM, %J Journal of Forensic Sciences: **Estimating Time Since Death from Postmortem Human Gut Microbial Communities**. 2015, **60**(5):1234–1240.
11. Debruyn JM, Hauther KAJP: **Postmortem succession of gut microbial communities in deceased humanÂ subjects**. 2017, **5**(6):e3437.
12. Zhang J, Wang M, Qi X, Shi L, Zhang J, Zhang X, Yang T, Ren J, Liu F, Zhang G, et al. Predicting the postmortem interval of burial cadavers based on microbial community succession. Forensic Sci International: Genet. 2021;52:102488.
13. Gulnaz J, Sheree, Finley, Zain, Abidin, Jennifer, Microbiology GJFi: **The Thanatomicrobiome: A Missing Piece of the Microbial Puzzle of Death**. 2016.
14. Burcham ZM, Hood JA, Pechal JL, Krausz KL, Bose JL, Schmidt CJ, Benbow ME, Jordan HR. Fluorescently labeled bacteria provide insight on post-mortem microbial transmigration. Forensic Sci Int. 2016;264:63–9.
15. Javan GT, Finley SJ, Can I, Wilkinson JE, Hanson JD, Tarone AMJSR: **Human Thanatomicrobiome Succession and Time Since Death**. 2016, **6**:29598.
16. Rakoff-Nahoum S, Foster KR, Comstock LE. The evolution of cooperation within the gut microbiota. Nature. 2016;533(7602):255–9.
17. Metcalf JL. Estimating the postmortem interval using microbes: Knowledge gaps and a path to technology adoption. Forensic Sci Int Genet. 2019;38:211–8.

18. Lawrence KE, Lam KC, Morgun A, Shulzhenko N, Löhr CV. Effect of temperature and time on the thanatomicrobiome of the cecum, ileum, kidney, and lung of domestic rabbits. J Vet Diagn Invest. 2019;31(2):155–63.
19. Howard GT, Norton WN, Stroot PG, Bailey KL, Watson EJ. Association of the genus Acinetobacter with the decomposition of a swine carcass and the isolation and characterization of a novel strain of Acinetobacter sp. P4. Curr Microbiol. 2012;64(1):24–33.
20. Kour D, Rana KL, Kumar R, Yadav N, Rastegari AA, Yadav AN, Singh K: Chap. 1 - **Gene Manipulation and Regulation of Catabolic Genes for Biodegradation of Biphenyl Compounds**. In: *New and Future Developments in Microbial Biotechnology and Bioengineering.* Edited by Singh HB, Gupta VK, Jogaiah S. Amsterdam: Elsevier; 2019: 1–23.
21. Newton RJ, Jones SE, Eiler A, McMahon KD, Bertilsson S. A guide to the natural history of freshwater lake bacteria. Microbiol Mol biology reviews: MMBR. 2011;75(1):14–49.
22. Schell MA, Karmirantzou M, Snel B, Vilanova D, Berger B, Pessi G, Zwahlen MC, Desiere F, Bork P, Delley M, et al: **The genome sequence of Bifidobacterium longum reflects its adaptation to the human gastrointestinal tract**. *Proceedings of the National Academy of Sciences of the United States of America* 2002, **99**(22):14422–14427.
23. Liedert C, Peltola M, Bernhardt J, Neubauer P, Salkinoja-Salonen M. Physiology of resistant Deinococcus geothermalis bacterium aerobically cultivated in low-manganese medium. J Bacteriol. 2012;194(6):1552–61.
24. Xie C-H, Yokota A. Sphingomonas azotifigens sp. nov., a nitrogen-fixing bacterium isolated from the roots of Oryza sativa. Int J Syst Evol MicroBiol. 2006;56:889–93.
25. Joshi KK, Chien P. Regulated Proteolysis in Bacteria: Caulobacter. Annu Rev Genet. 2016;50:423–45.
26. Kertesz* MA, Kawasaki A: **Hydrocarbon-Degrading Sphingomonads**: **Sphingomonas**, **Sphingobium**, **Novosphingobium**, **and Sphingopyxis**. In: *Handbook of Hydrocarbon and Lipid Microbiology.* Edited by Timmis KN. Berlin, Heidelberg: Springer Berlin Heidelberg; 2010: 1693–1705.
27. Kanazawa H, Ozaki S, Doi Y, Masuo S, Takaya N. Symbiotic riboflavin degradation by Microbacterium and Nocardioides bacteria. Biosci Biotechnol Biochem. 2020;84(5):1056–61.
28. Iancu L, Junkins EN, Necula-Petrareanu G, Purcarea CJeR. **Characterizing forensically important insect and microbial community colonization patterns in buried remains**. 2018, 8(1).
29. Galitskaya P, Biktasheva L, Saveliev A, Grigoryeva T, Boulygina E, Selivanovskaya S. Fungal and bacterial successions in the process of co-composting of organic wastes as revealed by 454 pyrosequencing. PLoS ONE. 2017;12(10):e0186051.
30. Lutz H, Vangelatos A, Gottel N, Osculati A, Visona S, Finley SJ, Gilbert JA, Javan GT. Effects of Extended Postmortem Interval on Microbial Communities in Organs of the Human Cadaver. Front Microbiol. 2020;11:569630–0.
31. Emmons AL, Mundorff AZ, Keenan SW, Davoren J, Andronowski J, Carter DO, DeBruyn JM. **Patterns of microbial colonization of human bone from surface-decomposed remains**. bioRxiv 2019:664482.

32. Hyde ER, Haarmann DP, Lynne AM, Bucheli SR, Petrosino JF. The living dead: bacterial community structure of a cadaver at the onset and end of the bloat stage of decomposition. PLoS ONE. 2013;8(10):e77733–3.
33. Li H, Yang E, Zhang S, Zhang J, Yuan L, Liu R, Ullah S, Wang Q, Mushtaq N, Shi Y, et al. Molecular characterization of gut microbial shift in SD rats after death for 30 days. Arch Microbiol. 2020;202(7):1763–73.
34. Yu Q, Zhou R, Wang Y, Feng T, Li H. Corpse decomposition increases nitrogen pollution and alters the succession of nirK-type denitrifying communities in different water types. Sci Total Environ. 2020;747:141472.
35. Masuda S, Bao Z, Okubo T, Sasaki K, Ikeda S, Shinoda R, Anda M, Kondo R, Mori Y, Minamisawa K. Sulfur Fertilization Changes the Community Structure of Rice Root-, and Soil- Associated Bacteria. Microbes and environments. 2016;31(1):70–5.
36. Dong K, Xin Y, Cao F, Huang Z, Sun J, Peng M, Liu W, Shi P. Succession of oral microbiota community as a tool to estimate postmortem interval. Sci Rep. 2019;9(1):13063.
37. Zhang B, Kong W, Wu N, Zhang Y. Bacterial diversity and community along the succession of biological soil crusts in the Gurbantunggut Desert, Northern China. J Basic Microbiol. 2016;56(6):670–9.
38. Roh H, Chu KH. Effects of solids retention time on the performance of bioreactors bioaugmented with a 17β-estradiol-utilizing bacterium, Sphingomonas strain KC8. Chemosphere. 2011;84(2):227–33.
39. Harrison L, Kooienga E, Speights C, Tomberlin J, Lashley M, Barton B, Jordan H. Microbial succession from a subsequent secondary death event following mass mortality. BMC Microbiol. 2020;20(1):309.
40. Chen J, Berry MJ. **Selenium and selenoproteins in the brain and brain diseases**. 2003, 86(1):1–12.
41. Yoshikawa T, Nakamura T, Yanai K. Histamine N-Methyltransferase in the Brain. Int J Mol Sci. 2019;20(3):737.
42. Micali G, Endres RG. Bacterial chemotaxis: information processing, thermodynamics, and behavior. Curr Opin Microbiol. 2016;30:8–15.
43. Leonardi R, Jackowski S. Biosynthesis of Pantothenic Acid and Coenzyme **A**. EcoSal Plus 2007, 2(2):10.1128/ecosalplus.1123.1126.1123.1124.
44. Gillner DM, Becker DP, Holz RC. Lysine biosynthesis in bacteria: a metallodesuccinylase as a potential antimicrobial target. J Biol Inorg Chem. 2013;18(2):155–63.
45. Pacheco-Alvarez D, Solórzano-Vargas RS, Del Río AL. Biotin in Metabolism and Its Relationship to Human Disease. Arch Med Res. 2002;33(5):439–47.
46. Spalding MD, Prigge ST. **Lipoic Acid Metabolism in Microbial Pathogens**. 2010, 74(2):200–228.
47. Tang K-H, Tang YJ, Blankenship RE. Carbon metabolic pathways in phototrophic bacteria and their broader evolutionary implications. Front Microbiol. 2011;2:165–5.

48. Bolyen E, Rideout JR, Dillon MR, Bokulich NA, Abnet CC, Al-Ghalith GA, Alexander H, Alm EJ, Arumugam M, Asnicar F, et al: **Reproducible, interactive, scalable and extensible microbiome data science using QIIME 2** (**vol 37, pg 852**, 2019). *Nature biotechnology* 2019, **37**(9):1091–1091.
49. Martin M: **Cutadapt removes adapter sequences from high-throughput sequencing reads**. 2011 2011, **17**(1):3%J EMBnet.journal.
50. Callahan B, McMurdie P, Rosen M, Han A, Johnson AJ, Holmes S. **DADA2: High-resolution sample inference from Illumina amplicon data**. Nature Methods 2016, 13.
51. Katoh K, Standley DM. MAFFT multiple sequence alignment software version 7: improvements in performance and usability. Mol Biol Evol. 2013;30(4):772–80.
52. Price MN, Dehal PS, Arkin AP. FastTree 2–approximately maximum-likelihood trees for large alignments. PLoS ONE. 2010;5(3):e9490–0.
53. Bokulich NA, Kaehler BD, Rideout JR, Dillon M, Bolyen E, Knight R, Huttley GA, Gregory Caporaso J. Optimizing taxonomic classification of marker-gene amplicon sequences with QIIME 2's q2-feature-classifier plugin. Microbiome. 2018;6(1):90.
54. Chao A. Non-parametric estimation of the classes in a population. Scand J Stat. 1984;11:265–70.
55. Shannon CE. A Mathematical Theory of Communication. Bell Syst Tech J. 1948;27(3):379–423.
56. Simpson EH. Measurement of Diversity. Nature. 1949;163(4148):688–8.
57. Faith DP. Conservation evaluation and phylogenetic diversity. Biol Conserv. 1992;61(1):1–10.
58. Pielou EC. The measurement of diversity in different types of biological collections. J Theor Biol. 1966;13:131–44.
59. Good IJ. THE POPULATION FREQUENCIES OF SPECIES AND THE ESTIMATION OF POPULATION PARAMETERS. Biometrika. 1953;40(3–4):237–64.
60. Lozupone CA, Hamady M, Kelley ST, Knight R. **Quantitative and Qualitative β Diversity Measures Lead to Different Insights into Factors That Structure Microbial Communities**. 2007, 73(5):1576–1585.
61. Lozupone C, Knight RJAEM. **UniFrac: a new phylogenetic method for comparing microbial communities**. 2005, 71(12):8228–8235.
62. Ramette AJFme: **Multivariate analyses in microbial ecology**. 2007, **62**(2):142–160.
63. **Permutational Multivariate Analysis of Variance** (**PERMANOVA**). In: *Wiley StatsRef: Statistics Reference Online.* 1–15.
64. Huson DH, Mitra S, Ruscheweyh H-J, Weber N, Schuster SCJGr. **Integrative analysis of environmental sequences using MEGAN4**. 2011, 21(9):1552–1560.
65. Asnicar F, Weingart G, Tickle TL, Huttenhower C, Segata NJP. **Compact graphical representation of phylogenetic data and metadata with GraPhlAn**. 2015, 3:e1029.
66. Segata N, Izard J, Waldron L, Gevers D, Miropolsky L, Garrett WS, Huttenhower CJGb: **Metagenomic biomarker discovery and explanation**. 2011, **12**(6):R60.

67. Douglas GM, Maffei VJ, Zaneveld JR, Yurgel SN, Brown JR, Taylor CM, Huttenhower C, Langille MGI. PICRUSt2 for prediction of metagenome functions. Nat Biotechnol. 2020;38(6):685–8.

Tables

Table 1 Differential genera associated with different organs during decomposition based on Lefse analysis.

Group	Genera	P value/ LDA score at hour 0.5	P value/ LDA score at hour 4	P value/ LDA score at hour 8	P value/ LDA score at hour 12	trend[a]
Brain	Ochrobactrum	0.0041/ 4.9100	0.0402/ 4.8934	0.0042/ 4.7879	0.0100/ 4.6123	up
	Agrobacterium	0.0018/ 4.2848	0.0007/ 4.2821	0.0004/ 4.7662	0.0007/ 4.5610	up
	Leptothrix	0.0012/ 3.5893	0.0013/ 3.6662	0.0001/ 3.8906	0.0009/ 3.7786	up
	Aminobacter	0.0032/ 3.5617	0.0354/ 3.6697	0.0041/ 3.6722	0.0124/ 3.4371	up
	Bradyrhizobium	0.0024/ 3.5432	0.0014/ 3.5230	0.0034/ 3.5848	0.0228/ 3.3360	up
	Phyllobacterium	0.0029/ 3.3562	0.0009/ 3.4450	0.0038/ 3.5664	0.0005/ 3.2525	up
Heart	Sphingomonas	0.0033/ 4.2528	0.0022/ 4.4560	0.0003/ 4.4591	0.0006/ 4.5032	up
Kidney	Lysinibacillus	0.0040/ 3.3069	0.0008/ 3.4894	0.0021/ 3.2596	0.0007/ 3.1509	up
	Perlucidibaca	0.0035/ 3.6762	0.0007/ 4.1782	0.0002/ 3.8716	0.0003/ 4.2633	up
	Limnobacter	0.0004/ 3.7829	0.0024/ 4.2050	0.0029/ 3.7611	0.0159/ 4.1156	up

[a] The trend means that the relative abundance of the corresponding genus was increased or decreased compared to other organ group at the same PMI.

Figures

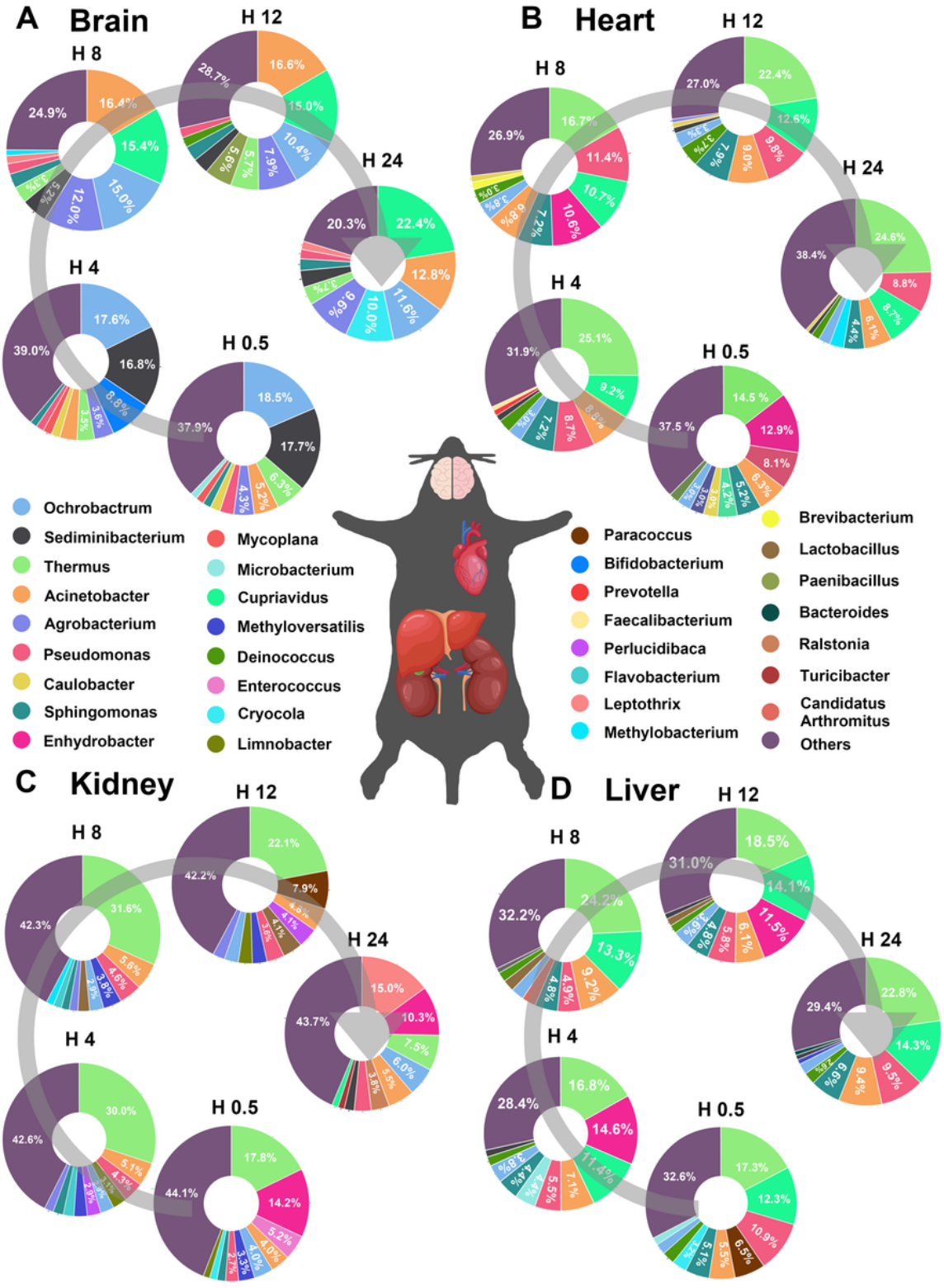

Figure 1

Mean relative abundance of the top 10 bacterial genera identified within each organ during 1 day of decomposition.

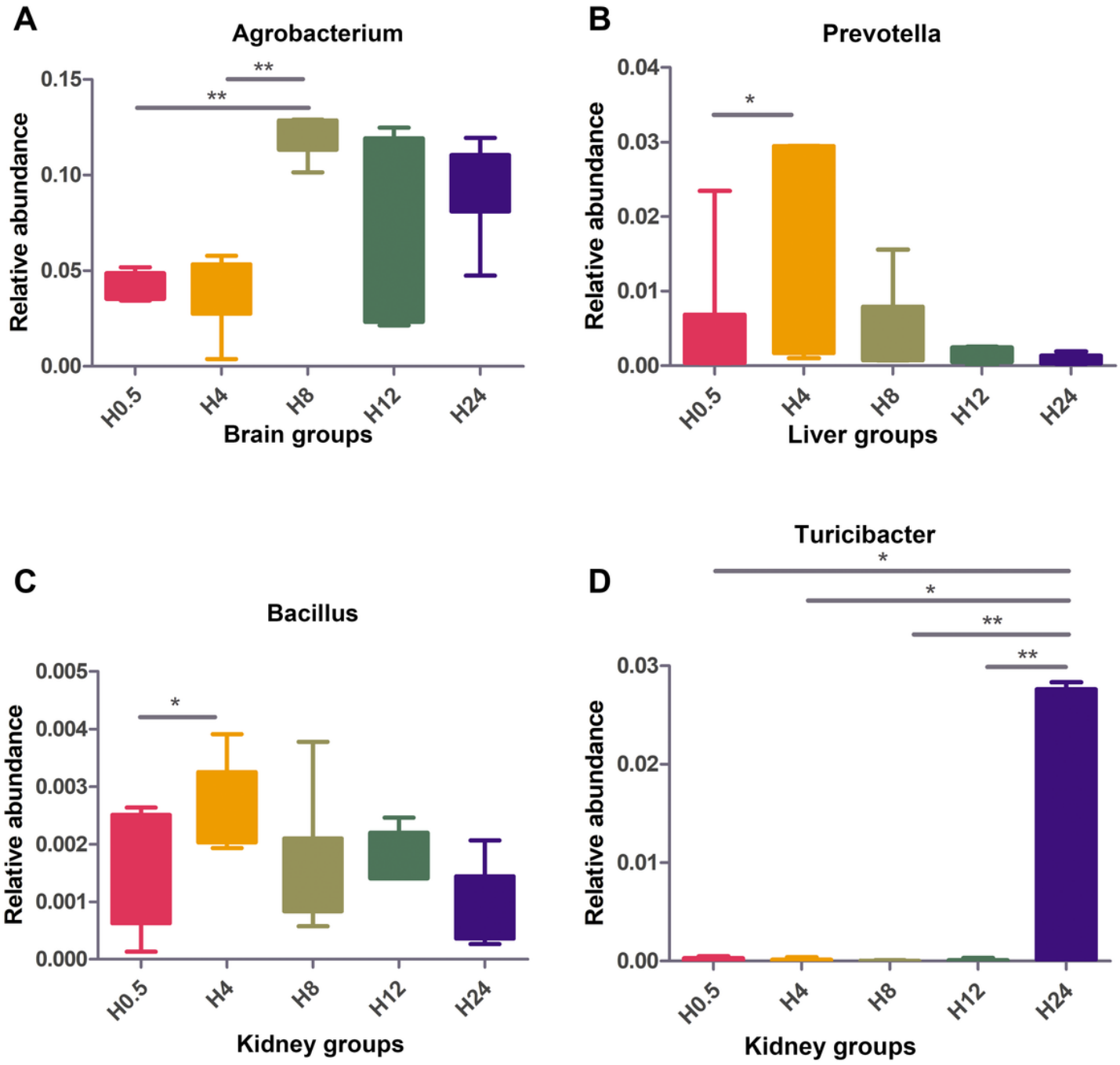

Figure 2

Significant relative abundance changes of some genera in postmortem organs (*P value< 0.05, **P value < 0.01, ***P value< 0.001, 6 samples per group).

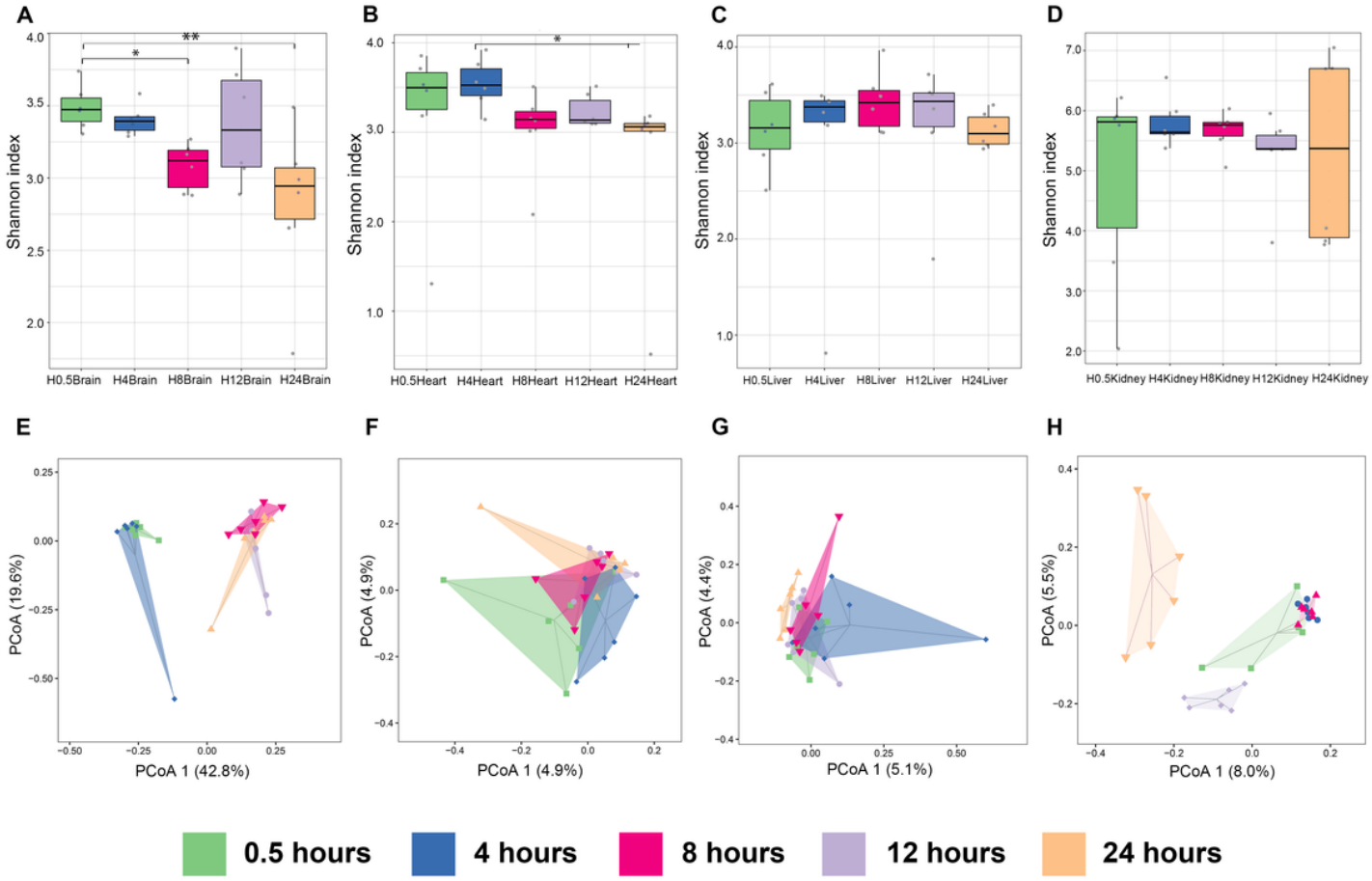

Figure 3

Alpha and beta diversity changed during 1-day decomposition. (A-D): Alpha diversity within subjects at different PMIs in different internal organs as measured using the Shannon index. *P value< 0.05, **P-value < 0.01, ***P value< 0.001, 6 samples per group. (E-H): PCoA plots based on weighted UniFrac distances of different postmortem groups in brain, heart, liver and kidney samples.

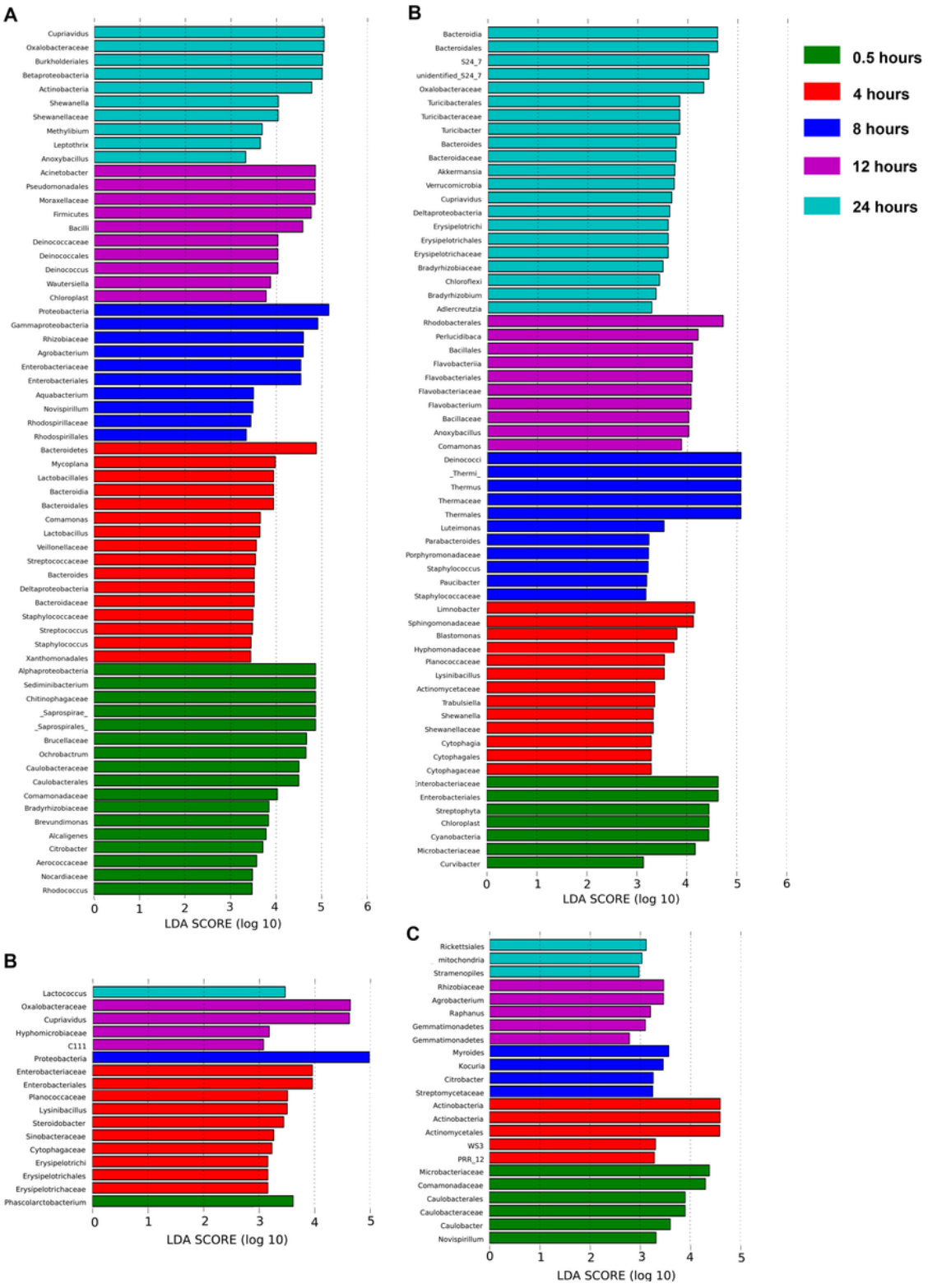

Figure 4

LEfSe rank plots of different organs among different decomposition stages. (A)-(D) Plots are representative of the brain, heart, liver, and kidney groups, respectively.

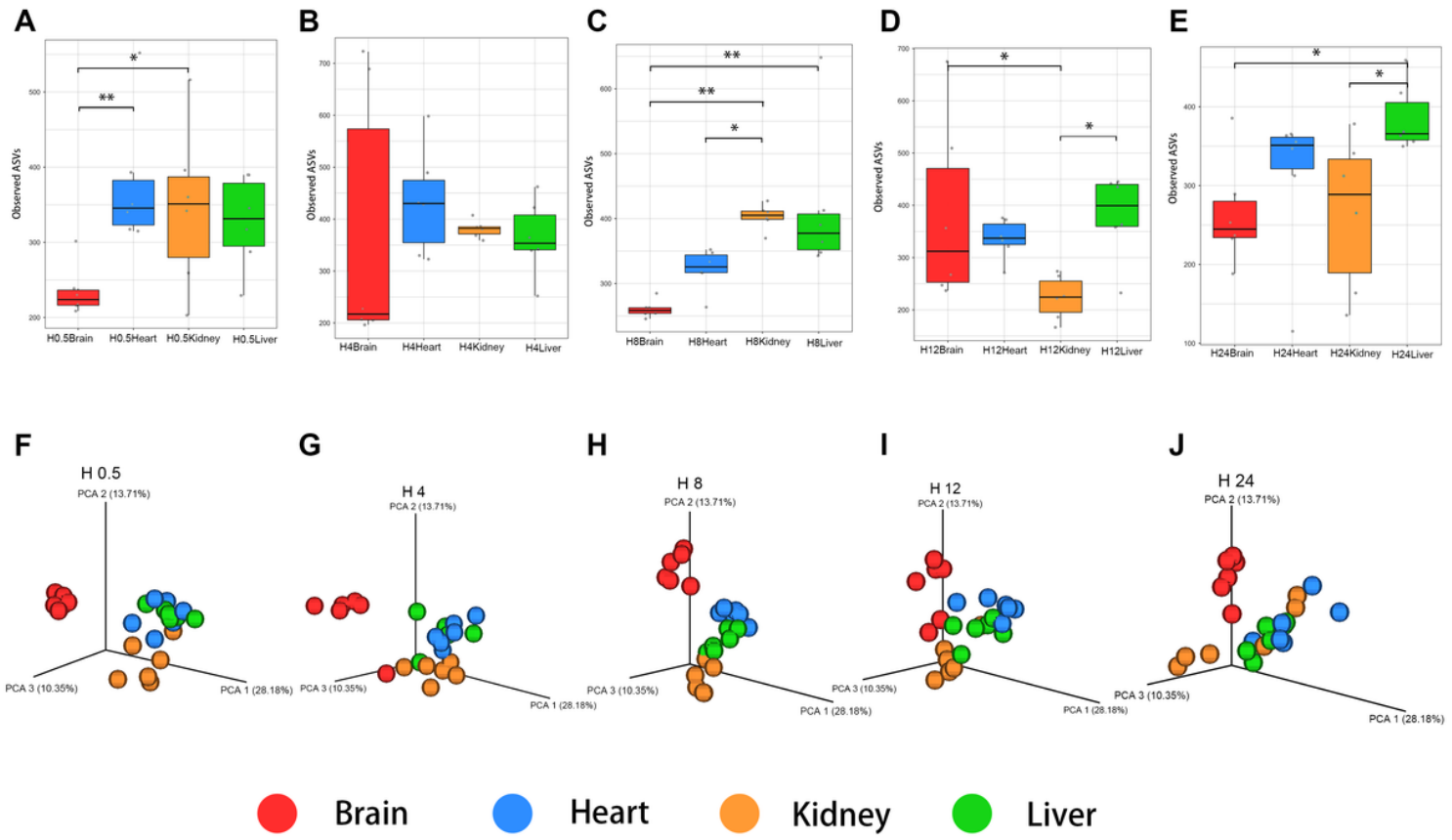

Figure 5

Alpha and beta diversity measures of microbial communities by organ. (A)-(E): Observed ASV richness by organ. *P< 0.05, **P< 0.01, ***P< 0.001; statistical methods: KW-test with Bonferroni correction or Student's t-test with Fisher's LSD; sample size: 6 samples per group. H0.5Brain v.s. H0.5Heart, P=0.005; H0.5Brain v.s. H0.5Kidney, P=0.025; H8Brain v.s.H8Kidney, P=0.001; H8Brain v.s. H8Liver, P=0.000; H8Heart v.s. H8Kidney, P=0.033; H12Brain v.s. H12Kidney, P=0.013; H12Kidney v.s. H12Liver, P=0.015; H24Brain v.s. H24Liver, P=0.031; H24Kidney v.s. H24Liver, P=0.031. (F)-(J): PCoA based on weighted UniFrac measures of microbial dissimilarity by organ.

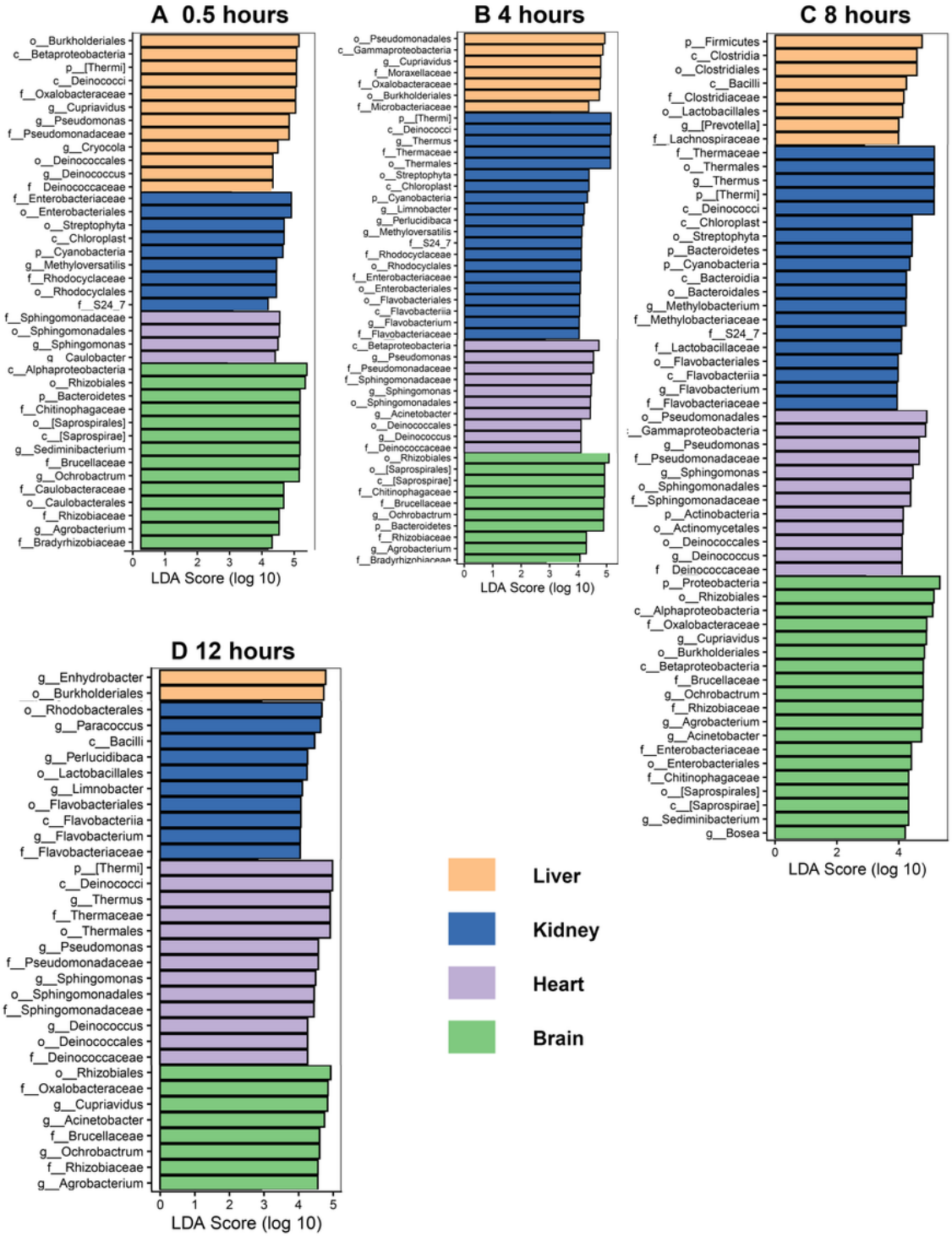

Figure 6

LEfSe analysis of the differential abundance of individual bacterial OTUs between each organ compared to all other organs at each PMI (the LDA threshold score was set as 4.0). (A)-(D): demonstrated the LEfSe results of 0.5, 4, 8, 12 hours after death, respectively.

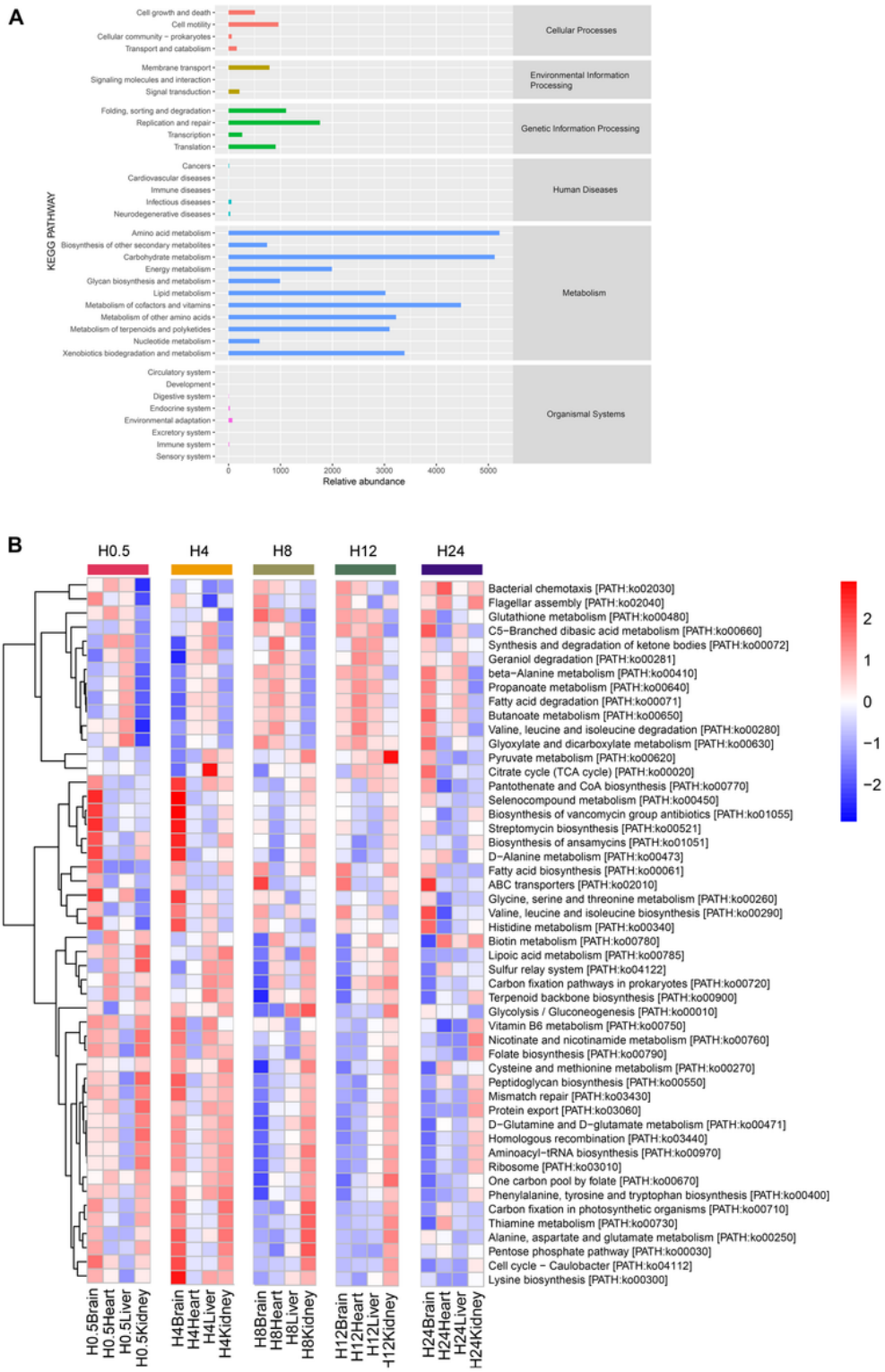

Figure 7

Predictive metabolic potential (from amplicon data) of postmortem internal organs. (A) Distribution of major metabolic KEGG categories across the samples. (B) Heatmap showing the distribution of genes based on level 2 KEGG orthologous gene identification by PICRUSt2 analysis.

Supplementary Files

This is a list of supplementary files associated with this preprint. Click to download.

- AuthorArriveChecklist.pdf
- figureS1.tif
- figureS2.tif
- figureS3.tif
- figureS4.tif